Surface Patterning

DOI: 10.1002/anie.200904993

Self-Assembly of Rodlike Bio-nanoparticles in Capillary Tubes**

Yuan Lin, Elizabeth Balizan, L. Andrew Lee, Zhongwei Niu, and Qian Wang**

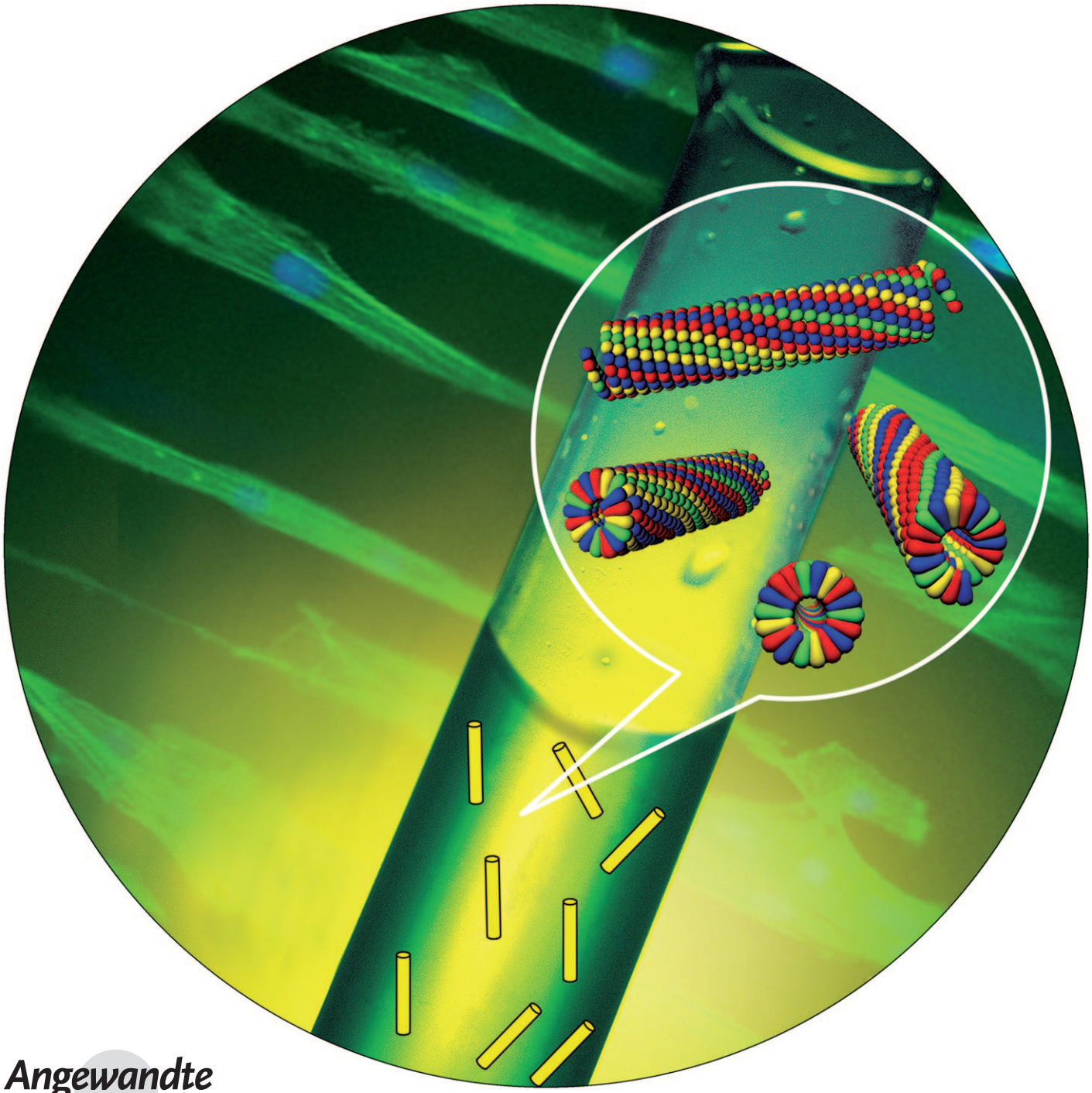

The alignment of nanoparticle building blocks into ordered hierarchical structures is very important in colloidal and materials chemistry.[1–2] Drying of nanoparticle suspensions is a relatively easy method that is used to fabricate large-scale patterns with well-defined superstructures.[2–4] The formation of a ringlike structure at the contact line when a suspension dries on a solid surface is an everyday phenomenon that has been widely used to create hierarchical patterned structures.[5] The contact line can stay pinned to form a single ring (i.e., "coffee ring")[3,5] or can shrink in a discontinuous manner to generate multiple rings.[6–8] This phenomenon can be used to tune the formation of different patterns in a confined geometry.[9–10] Basic theoretical studies have been performed to understand how different patterns are formed during the drying process.[3,9,11–13] In general, the pinning and depinning (stick–slip motion) at the contact line governs such pattern formation.[14] Spherical colloidal particle suspensions and polymer solutions are two widely used systems for theoretical and experimental studies. A systematic study of the orientation of anisotropic particles, such as nanorods, at the contact line during the drying process can further improve the theoretical understanding of pattern formation induced by solvent evaporation. From a practical point of view, such knowledge may lead to a facile method of patterning and alignment of rodlike particles, which is critical for applications such as thin-film transistors, molecular electronics, and biosensors.[15–20]

Herein, we report the formation of diverse patterns that result from drying a solution of rodlike tobacco mosaic virus (TMV) particles in a glass capillary tube. The tube was used to not only provide a confined space, but also to create a curved surface with multiple forces at the contact line to control the self-assembly process (Figure 1). TMV is an ideal candidate for these studies because of its rodlike morphology and high monodispersity. TMV has also been widely used as a model rodlike particle in self-assembly studies[21–22] and a basic building block for new materials development.[23]

In our experiments, TMV solutions were dried in a horizontal open-ended capillary tube (length 2.2 cm, inner diameter 0.15 cm) under ambient conditions (Figure 2a). Symmetrical patterns were formed around the interior of the tube (Figure 2b–i and Figure 3). Different patterns were generated because of the interfacial assembly of TMV particles at the air–liquid interface and a pinning–depinning process. The concentration of TMV, the salt concentration in aqueous solution, and the surface properties of the capillary tube interior are three key factors that govern such combined self-assembly behavior.

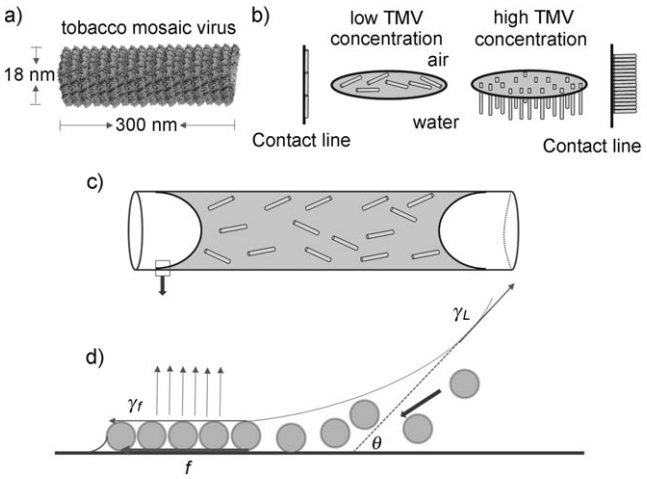

Figure 1. a) Crystal structure of TMV. Model generated using PyMol (www.pymol.org) with coordinates obtained from RCSB Protein Data Bank (www.pdb.org). b) TMV particles (represented as yellow rods) self-assemble at the air–liquid interface and the contact line. Left: TMV deposits parallel to the contact line at low TMV concentrations. Right: TMV deposits perpendicular to the contact line at high TMV concentration. c) Schematic representation of a capillary tube containing TMV solution. d) Schematic illustration of the thin meniscus formed at the contact line, as indicated in a small blue square in the lower left corner (c). TMV particles are represented as yellow dots. The red arrow on the left represents the direction of the frictional force f generated by the deposition of particles at the contact line. The thick blue arrow on the right represents the moving direction of TMV particles caused by the convective force. Two thin blue arrows represent γ_f and γ_L. θ is the contact angle between water and the substrate.

We first studied the pattern formation from various concentrations of TMV at fixed salt concentration (0.01M potassium phosphate buffer, pH 7.4; Figure S1 in the Supporting Information). With a TMV concentration of 0.01 mg mL^{-1}, stripe patterns were formed around the interior of the capillary tube. As the solution dried deeper within the capillary, the reduced water evaporation rate caused the distance between the two pinning lines to gradually increase (Figure 2b,c).[24] The height profile of the AFM image (Figure 2d) clearly shows that the band is only composed of a single layer of TMV particles. The particles form a close-packed structure, in which TMVs are oriented parallel to the contact line but perpendicular to the long axis of the capillary tube. Similar patterns were formed when the TMV concentration was increased to 0.1 mg mL^{-1} (Figure 2f–i); each band is composed of multilayers of TMV, which are also oriented parallel to the contact line. Upon further increasing the TMV concentration to 0.5 mg mL^{-1}, the entire capillary tube is covered with TMV, and no stripe patterns are observed, while most of TMVs are still aligned perpendicular to the long axis of the tube (although it is not a perfect pattern; Figure S1c in the Supporting Information). Zig-zag patterns are formed at TMV concentrations greater than 5 mg mL^{-1} (Figure S1d in the Supporting Information).

[*] Dr. Y. Lin, E. Balizan, L. A. Lee, Prof. Z. Niu,[+] Prof. Q. Wang
Department of Chemistry and Biochemistry and Nanocenter
University of South Carolina
631 Sumter St., Columbia, SC, 29208 (USA)
E-mail: niu.z@mail.chem.sc.edu
wang@mail.chem.sc.edu

[+] Current address: Technical Institute of Physics and Chemistry
Chinese Academy of Sciences, Beijing 100190 (China)

[**] We thank Dr. Yao Lin and Dr. Taixing Cui for helpful discussions. This work was supported by the US NSF (DMR-0706431, CHE-0748690), the Alfred P. Sloan Scholarship, the Camille Dreyfus Teacher Scholar Award, US-ARO-W911NF-09-1-236, and the W. M. Keck Foundation.

Supporting information for this article is available on the WWW under http://dx.doi.org/10.1002/anie.200904993.

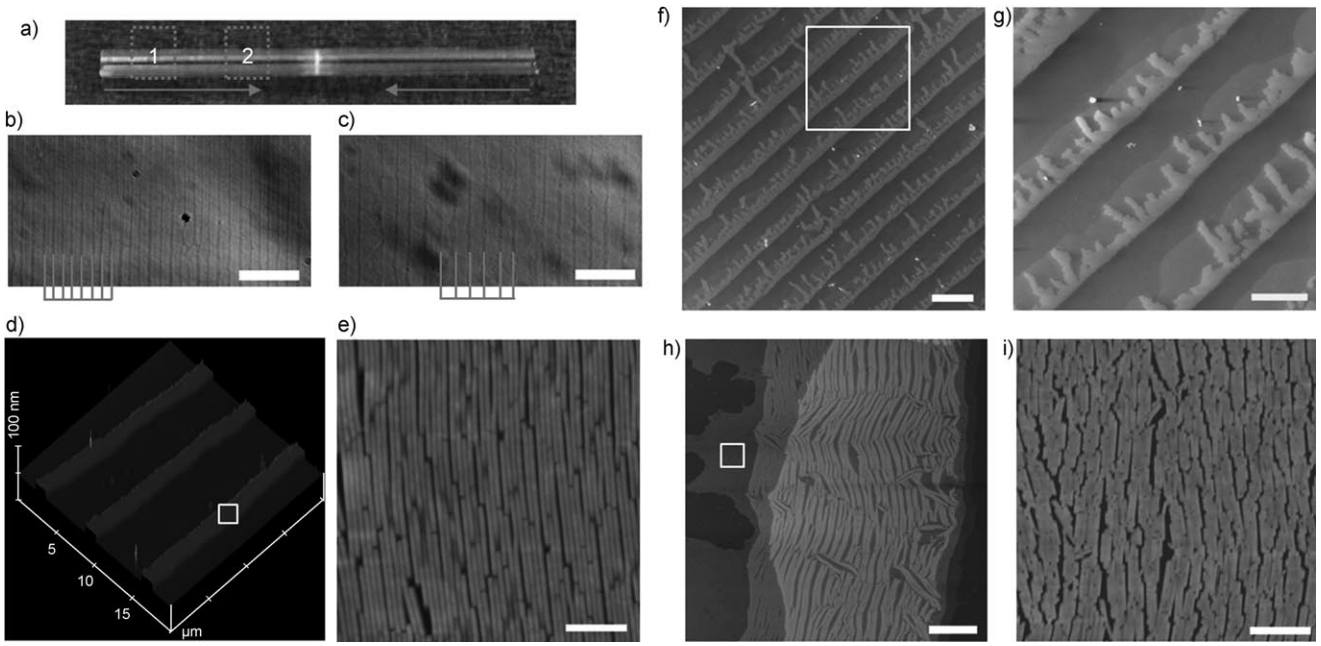

Figure 2. Patterns formed in a glass capillary tube after evaporation of different concentrations of TMV in a potassium phosphate buffer (0.01 M, pH 7.4). a) Glass capillary tube. Arrows indicate the drying direction and squares 1 and 2 represent two different areas of the tube. Optical images of stripe patterns formed at b) position 1 and c) position 2 in (a), respectively, after drying 0.01 mg mL^{-1} TMV solution in the capillary tube. d) 3D AFM image of stripe patterns shown in (b). e) An enlarged view of the square region enclosed by the white line in (d). f) Scanning electron microscopy (SEM) image of stripe patterns after drying 0.1 mg mL^{-1} TMV solution in a capillary tube. g) An enlarged view of the square region enclosed by the white line in (f). h) AFM image of single stripe shown in (g). i) An enlarged view of the square region enclosed by the white line in (h). Scale bars: b, c: 50 μm; e: 200 nm; f: 50 μm; g: 20 μm; h: 4 μm; i: 400 nm.

The formation of hierarchical structures is determined by the preferred orientation of TMV at the air–liquid interface as well as the pinning–depinning process. At low concentrations of TMV with salts, the TMV is oriented parallel to the plane of the interface to maximize the interfacial coverage per particle (Figure 1 b).[25] A thin meniscus is formed at the solid–liquid–vapor interface (contact line; Figure 1 c). As the water evaporates, convective transport drives TMV particles to the contact line and deposits TMV onto the substrate (Figure 1 d). The surface roughness is generated by the deposition of TMV particles to produce a frictional force f, which, together with the liquid surface tension γ_f pins the position of the contact line.[11] As the evaporation proceeds, the water will have more contact with TMV and less contact with the glass surface. The capillary force γ_L pulls the liquid inward, and the contact line becomes depinned. The contact line slips and reaches another equilibrium position, where the water is again in contact with the glass surface. Consequently, the process repeats periodically, and the resulting stick–slip motion forms the periodic pattern (see Movie 1 in the Supporting Information). At higher TMV concentrations, the salt screens the surface charge of the TMV, thus reducing the repulsion between of TMV particles (Figure S2 in the Supporting Information). As a result, the virus particles form bundles or aggregates. When these bundles deposit at the contact line, the generated frictional force f increases, together with the liquid surface tension γ_f, which is larger than the capillary force γ_L. Hence the contact line cannot be depinned, and no stripe patterns were observed.

The TMV concentration determines the amount of particles supplied to the stripe-growing region, which is directly related to the width and thickness of the stripes. A higher concentration of the TMV solution will drive more TMV particles to the tip of the meniscus, where the particle film grows, thus resulting in thicker and wider stripes. At higher concentrations of TMV ($0.05\ \text{mg mL}^{-1} < [\text{TMV}] < 0.5\ \text{mg mL}^{-1}$), a multilayer of TMV stripe patterns was formed. The width of the TMV stripes and adjacent spacing increases almost linearly against TMV concentration (Figure S3 in the Supporting Information). At low TMV concentrations ($0.01\ \text{mg mL}^{-1} < [\text{TMV}] < 0.05\ \text{mg mL}^{-1}$), monolayer stripes form and the stripe width increases linearly against the particle concentration. However, all the monolayer samples have the same stripe thickness, which results in equal-sized meniscuses and thus equal-sized adjacent spacings (Figure S4 in the Supporting Information).

If the salt is removed, the assembly behavior changes dramatically. Instead of stripes or zig-zag patterns, irregular aggregations of TMV are formed in the capillary tube at a TMV concentration of 0.01 mg mL^{-1} in pure water (Figure 3 a). Without a salt in solution to screen the charges, the overall negatively charged TMV particles (the isoelectric point (pI) of TMV is 3.4)[23] repel each other. As a result, when some TMV particles are deposited at the contact line, other virus particles are repelled. No regular patterns can be formed in this situation. At a TMV concentration of 0.1 mg mL^{-1}, the air–liquid interface is saturated with randomly packed viral particles; therefore, TMV randomly deposits on the substrate

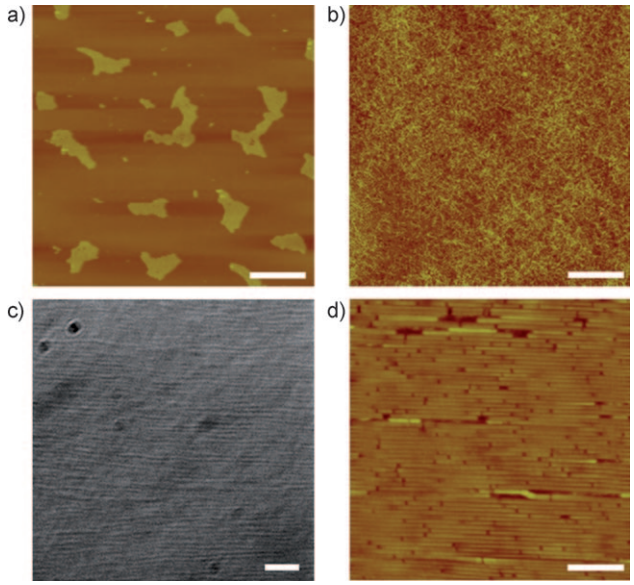

Figure 3. AFM images of drying TMV solution in the capillary tube with TMV concentration of a) 0.01 mg mL^{-1} and b) 0.1 mg mL^{-1}. c) Optical and d) AFM images of drying 26 mg mL^{-1} TMV solution in the capillary tube. Scale bars: a, b: 4 μm; c: 10 μm; d: 200 nm.

and forms a loose multilayer structure (Figure 3b). A further increase in the TMV concentration will increase the volume fraction of TMV at the interface, thus leading to an increase in the dipole–dipole repulsion between TMV rods until they are forced to orient perpendicular to the air–liquid interface (Figure 1b). The rodlike particles not only relieve the strong dipole–dipole repulsion, but also effectively minimize the interfacial energy.[25] As well as the repulsive force, a long-range capillary force, which comes from the deformation of the meniscus between two particles, can help maintain the long-range order of the particles at the liquid–liquid interface.[26] Therefore, upon deposition at the contact line, a continuous TMV thin film can be prepared with the virus oriented perpendicular to the contact line but parallel to the long axis of the capillary tube (Figure 3c,d, see also Movie 2 in the Supporting Information).

As well as the concentration and salt effects, the surface properties of the capillary interior surface play an important role in the pattern formation. In order to form a stripe pattern, the contact angle between water and the substrate must be smaller than the contact angle between water and TMV ($\theta_{tmv} = (40 \pm 3)°$). For example, the contact angle between water and clean glass θ_{glass} is $(10 \pm 3)°$. To confirm this condition, two substrates, coated with poly(styrenesulfonic acid) (PSS) and a mixture of PSS/sodium dodecyl sulfate (SDS; 1:5) respectively, were prepared through a layer-by-layer method. TMV formed similar stripe patterns on the PSS-coated surface, which has a contact angle of $(24 \pm 2)°$—smaller than that of TMV. In comparison, on a PSS/SDS-modified surface, which has a contact angle of $(60 \pm 2)°$—larger than that of TMV—the contact line cannot be pinned, and the capillary force drives TMVs inside the tube. Most of TMVs were found in the middle part of the capillary tube (data not shown).

One direct application of the patterned structure in the capillary tube is to direct the orientation of the smooth muscle cells (SMCs) perpendicular to the long axis of the tube. In the body, SMCs are spindle-shaped and align their long axis perpendicular to the blood vessel length. This orientation is

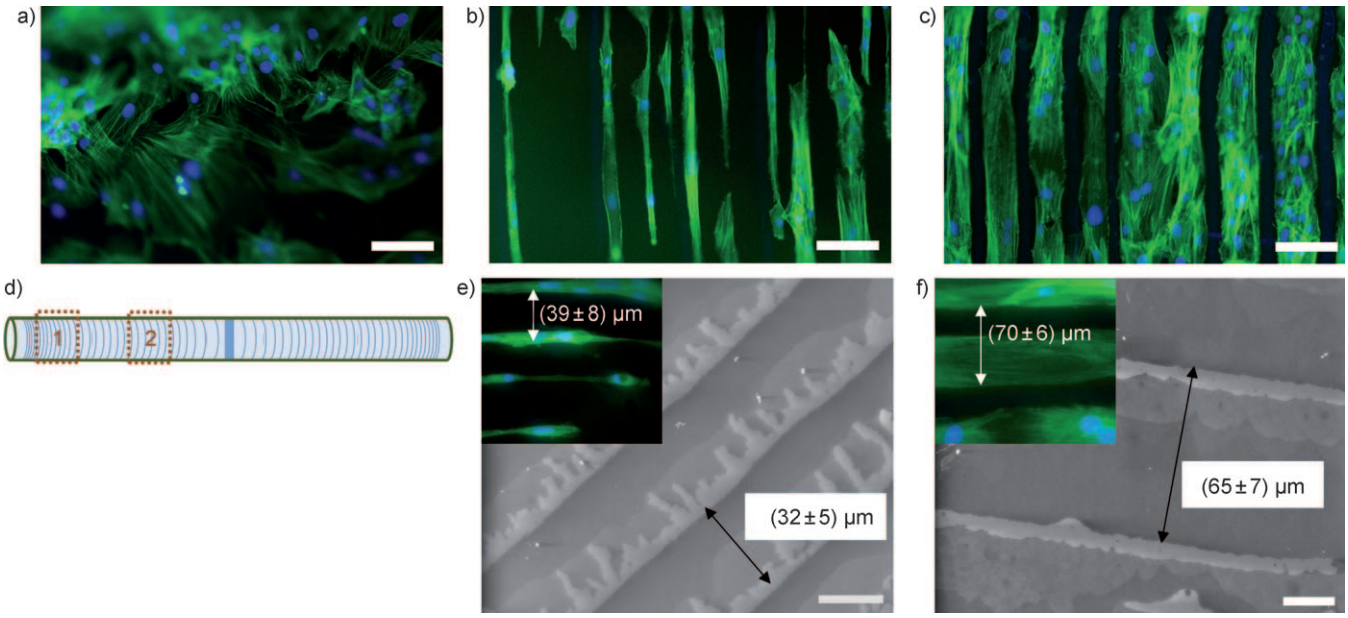

Figure 4. Rat aortic smooth muscle cells cultured in capillary tubes. a) Florescence images of SMCs cultured in a blank glass capillary tube. Florescence images of SMCs cultured at b) position 1 and c) position 2 in (d) inside the capillary tube. d) Schematic illustration of the capillary tube with stripe TMV patterns. SEM images of stripe patterns at e) position 1 and f) position 2 in (d). The insets show the fluorescence images of SMCs cultured inside the capillary at the same location as (e) and (f), which share similar distances between two stripes. Scale bars: a–c: 50 μm; e, f: 20 μm.

crucial for proper blood vessel function. In a diseased or damaged blood vessel, SMCs change to a synthetic phenotype and exhibit an increased proliferation rate. Most efforts have focused on either stress-induced SMC alignment or 2D patterns generated by lithography or mechanical stress.[27–28] In contrast to the SMCs cultured in glass capillary tubes (Figure 4a), SMCs cultured inside the TMV-patterned capillary tubes align perpendicular to the capillary tube (Figure 4b,c). In glass capillary tubes without TMV patterns (Figure 4a), the morphology of SMCs was epithelioid or rhomboid, which is typical of the pathogenic synthetic phenotype.[29] However, SMCs cultured in the tube with stripe patterns tended to be spindle-shaped, which is typical of the contractile phenotype (Figure 4b,c). The distance between cell stripes is consistent with that of TMV stripe patterns along the capillary tube (Figure 4e,f). By light microscopy alone, it is difficult to discern whether SMCs grow on the TMV ridge surface or between TMV stripes on the glass surface. To address this question, fluorescently tagged TMV (FL-TMV) was deposited inside the capillary tube in the same manner as the wide-type TMV. After culturing SMCs in the capillary tube with the FL-TMV, SMCs can be seen growing in the glass groove part of the tube instead of on top of the TMVs (see Figure S5 in the Supporting Information).

As a control system, bovine serum albumin (BSA) was assembled by following the same protocol as for TMV in the capillary tube to afford a similar stripe pattern. After culturing SMCs in the BSA-patterned capillary tube, cells can also grow into an aligned pattern (Figure S6 in the Supporting Information). This technique can therefore be applied to other types of capillary tubes and other biomacromolecules, therefore it has great potential in the development of enhanced vascular grafts.

Received: September 6, 2009
Published online: December 9, 2009

Keywords: nanostructures · self-assembly · surface analysis · surface patterning · tobacco mosaic virus

[1] W. Cheng, N. Park, M. T. Walter, M. R. Hartman, D. Luo, *Nat. Nanotechnol.* **2008**, *3*, 682 – 690.
[2] O. D. Velev, S. Gupta, *Adv. Mater.* **2009**, *21*, 1897 – 1905.
[3] R. D. Deegan, O. Bakajin, T. F. Dupont, G. Huber, S. R. Nagel, T. A. Witten, *Phys. Rev. E* **2000**, *62*, 756 – 765.
[4] J. Huang, F. Kim, A. R. Tao, S. Connor, P. Yang, *Nat. Mater.* **2005**, *4*, 896 – 900.
[5] R. D. Deegan, O. Bakajin, T. F. Dupont, G. Huber, S. R. Nagel, T. A. Witten, *Nature* **1997**, *389*, 827 – 829.
[6] S. Maheshwari, L. Zhang, Y. Zhu, H. C. Chang, *Phys. Rev. Lett.* **2008**, *100*, 044503.
[7] L. Shmuylovich, A. Q. Shen, H. A. Stone, *Langmuir* **2002**, *18*, 3441 – 3445.
[8] S. W. Hong, M. Byun, Z. Lin, *Angew. Chem.* **2009**, *121*, 520 – 524; *Angew. Chem. Int. Ed.* **2009**, *48*, 512 – 516.
[9] J. Xu, J. Xia, S. W. Hong, Z. Lin, F. Qiu, Y. Yang, *Phys. Rev. Lett.* **2006**, *96*, 066104.
[10] Z. Lin, S. Granick, *J. Am. Chem. Soc.* **2005**, *127*, 2816 – 2817.
[11] P. G. De Gennes, *Rev. Mod. Phys.* **1985**, *57*, 827 – 863.
[12] A. S. Dimitrov, K. Nagayama, *Langmuir* **1996**, *12*, 1303 – 1311.
[13] N. D. Denkov, O. D. Velev, P. A. Kralchevsky, I. B. Ivanov, H. Yoshimura, K. Nagayama, *Langmuir* **1992**, *8*, 3183 – 3190.
[14] E. Adachi, A. S. Dimitrov, K. Nagayama, *Langmuir* **1995**, *11*, 1057 – 1060.
[15] Z. Nie, D. Fava, E. Kumacheva, S. Zou, G. C. Walker, M. Rubinstein, *Nat. Mater.* **2007**, *6*, 609 – 614.
[16] M. Engel, J. P. Small, M. Steiner, M. Freitag, A. A. Green, M. C. Hersam, P. Avouris, *Acs Nano* **2008**, *2*, 2445 – 2452.
[17] R. Sharma, M. S. Strano, *Adv. Mater.* **2009**, *21*, 60 – 65.
[18] H. Nakamura, X. Li, H. Wang, M. Uehara, M. Miyazaki, H. Shimizu, H. Maeda, *Chem. Eng. J.* **2004**, *101*, 261 – 268.
[19] K. T. Nam, D. W. Kim, P. J. Yoo, C. Y. Chiang, N. Meethong, P. T. Hammond, Y. M. Chiang, A. M. Belcher, *Science* **2006**, *312*, 885 – 888.
[20] J. Rong, L. A. Lee, K. Li, B. Harp, C. M. Mello, Z. Niu, Q. Wang, *Chem. Commun.* **2008**, 5185 – 5187.
[21] D. M. Kuncicky, R. R. Naik, O. D. Velev, *Small* **2006**, *2*, 1462 – 1466.
[22] a) M. Adams, S. Fraden, *Biophys. J.* **1998**, *74*, 669 – 677; b) Z. Dogic, S. Fraden, *Curr. Opin. Colloid Interface Sci.* **2006**, *11*, 47 – 55.
[23] Z. Niu, J. Liu, L. A. Lee, M. A. Bruckman, D. Zhao, G. Koley, Q. Wang, *Nano Lett.* **2007**, *7*, 3729 – 3733.
[24] M. Abkarian, J. Nunes, H. A. Stone, *J. Am. Chem. Soc.* **2004**, *126*, 5978 – 5979.
[25] J. He, Z. Niu, R. Tangirala, J. Y. Wang, X. Wei, G. Kaur, Q. Wang, G. Jutz, A. Boker, B. Lee, S. V. Pingali, P. Thiyagarajan, T. Emrick, T. P. Russell, *Langmuir* **2009**, *25*, 4979 – 4987.
[26] M. G. Nikolaides, A. R. Bausch, M. F. Hsu, A. D. Dinsmore, M. P. Brenner, C. Gay, D. A. Weitz, *Nature* **2002**, *420*, 299 – 301.
[27] P. Zorlutuna, A. Elsheikh, V. Hasirci, *Biomacromolecules* **2009**, *10*, 814 – 821.
[28] R. De, A. Zemel, S. A. Safran, *Nat. Phys.* **2007**, *3*, 655 – 659.
[29] G. K. Owens, M. S. Kumar, B. R. Wamhoff, *Physiol. Rev.* **2004**, *84*, 767 – 801.

